Optical Lenses for Atomic Beams

Ole Steuernagel

School of Physics, Astronomy and Mathematics,

University of Hertfordshire, Hatfield, AL10 9AB, UK *

(Dated: January 14, 2009)

Abstract

Superpositions of paraxial laser beam modes to generate atom-optical lenses based on the optical dipole force are investigated theoretically. Thin, wide, parabolic, cylindrical and circular atom lenses with numerical apertures much greater than those reported in the literature to date can be synthesized. This superposition approach promises to make high quality atom beam imaging and nano-deposition feasible.

PACS numbers: 37.10.Vz, 32.80.Qk,

*Electronic address: O.Steuernagel@herts.ac.uk

I. INTRODUCTION

The field of atom-optics offers considerable potential in applied and fundamental physics, both for atom beam lithography (to create nano-structures) [1, 2] and for atom beam microscopy [3, 4]. Here, the use of the optical dipole force using far detuned laser light for the manipulation of neutral atoms is considered. In this regime it yields a conservative potential for the manipulation of atoms that is proportional to the laser light intensity [1, 5].

Already in 1978 Ashkin's group demonstrated neutral atom beam focusing using the optical dipole force [6]. Many techniques to focus atomic beams have been tried since: mirrors [7, 8], transmission gratings [9, 10], holographic reflection-gratings [11], electro-static lenses [12], magnetic lenses [1, 13, 14, 15, 16] or magnetic mirrors [17], nano-apertures [18, 19, 20], and optical setups [1, 6, 18, 20, 21, 22, 23, 24, 25, 26, 27, 28, 29, 30, 31] relying on the optical dipole force [1, 5].

Amongst optical dipole force approaches there are schemes based on pulsed laser configurations [21, 22], light confined by nano-apertures [18], single-mode hollow beams [6, 23, 24] or standing wave setups that yield tightly spaced ridges of the atomic deposition patterns [1, 25, 26, 27, 28]. Standing wave pattern approaches can also yield other deposition patterns [29, 30], but because of the high spatial frequencies involved, smooth profiles such as those desired for aberration-free atom-lenses wider than 200 nm cannot be synthesized with this approach [1, 26, 30, 31].

In the case of standing wave setups [1, 30] spherical aberrations give rise to pronounced pedestals, filling the gaps between patterned areas [1, 25, 30]. This makes it impossible to lay down separate nano-wires. A pulsed approach should reduce the pedestal problem [32] but remains constrained by the short spatial wavelengths typical for standing wave approaches [33]. A related approach [27], that suffers less from pedestal problems, uses atomic de-excitation processes creating an effective transmission mask for excited noble-gas atoms to etch structures. Unfortunately, it appears to be unsuitable for direct deposition of metal atoms (they tend to stick to the deposition area regardless of their internal state). Its inherent filtering reduces atomic deposition rates and, more importantly, it does not redirect the center of mass of atomic motion and thus cannot be used for traditional imaging of atomic beams.

Similar problems occur in the application of single-mode hollow laser beams [23, 24] as

optical imaging elements. Their waist is potentially wide, but their elongation leads to thick lenses with small numerical apertures: for realistic setups a diameter of the transverse parabolic part of the potential of less than 200 nm arises in conjunction with focal lengths in the micrometer range [18, 23, 24] yielding unsatisfactorily small numerical apertures for atomic focussing. This implies that one would have to start out with already well focussed atomic beams and, yet, the resulting atomic point-spread function remains unsuitably wide. None of the approaches mentioned so far has been adopted as a solution for the problem of imaging of atomic beams in atomic microscopy [3, 4] or direct atom-deposition lithography [1, 2]: a viable atom-optical lens still needs to be found.

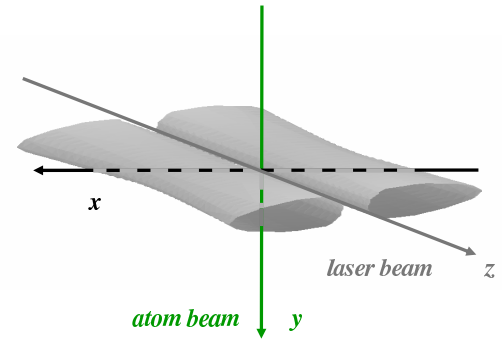

FIG. 1: (Color online) Arrangement of beams.

Here, it is shown that only the superposition of many laser modes [34, 35, 36] will allow us to generate wide atom-optical lenses based on the optical dipole force. We will find that widening the beams' waists is not a solution if atomic lenses with large numerical apertures are desired, because prohibitive increases in laser power are necessary. The idea of this paper is to superpose several odd Hermite-Gaussian TEM$_{mn}$-modes, $\psi_{m,n}$ [37, 38, 39], such that all non-linear terms in the dependence of the electric field on the (transverse) x-direction are optimally suppressed, see Fig. 1. This generates an electric field profile that varies linearly across a large part of the laser beam's cross section, see Fig. 2, and yields the desired parabolic laser intensity profile to generate an aberration-free atom-optical lens.

After an introduction of the underlying idea in Section II, its possible implementation using Hermite-Gaussian modes to generate cylindrical lenses is described in Section III. Section IV generalizes this approach to a crossed beam configuration that yields thin spherical lenses. We conclude in Section V.

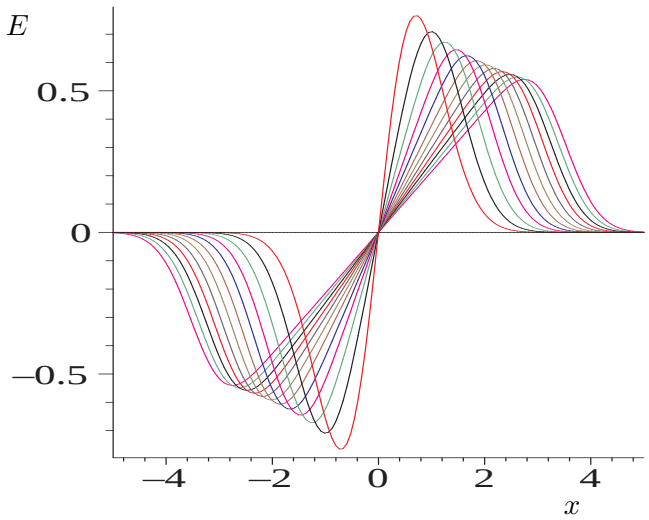

FIG. 2: (Color online) Electric field profile, $E_{2J+1}(x,0,0)$, at focal cross-section of Hermite-Gauss beams comprising superpositions of up to 23rd order odd modes (i.e. $2J+1=1,3,\ldots,23$; x-axis in units of beam waist w_{0x}, total cross-sectional beam power normalized to unity, Rayleigh lengths kept constant, $\epsilon_0\omega_L^2/2$ set to unity).

II. SUPERPOSITIONS OF ODD MODES

We now consider cylindrical atom-lenses with a parabolic modulation in the x-direction, see Fig. 1; most of what follows can be translated into the scenario of circular lenses for which atomic beams co-propagate with the focussing laser beams [6, 23] on their optical axis – instead of crossing through it. Such circular lenses would require the use of Laguerre-Gaussian instead of Hermite-Gaussian modes [23] but they have the disadvantage of yielding either tiny lenses (in the case of strongly focussed laser beams) or thick lenses (for less focussed laser beams) [23]. We therefore do not investigate setups with laser beams co-propagating with the atomic beam here; instead, we will show in Section IV how to create a thin spherical lens using a combination of two orthogonally crossed multimode Hermite-Gaussian laser beams.

A. Hermite-Gaussian modes

Let us consider modes, $\psi_{m,n}$ [37, 38, 39], with transverse beam coordinates x and y propagating in the z-direction. The Rayleigh lengths z_{R_x} and z_{R_y} associated with the two transverse coordinates, x and y, can be different from each other (focussed by different cylindrical lenses, say). In this case two different associated beam waist radii, w_{0x} and

w_{0y}, and Gouy-phases, $\phi_x(z)$ and $\phi_y(z)$ arise. In the paraxial approximation the normalized modes have the form

$$\begin{aligned}\psi_{m,n}(\boldsymbol{r}) = & \sqrt{\tfrac{\sqrt{2}}{w_x(z)}}\ \varphi_m\left(\tfrac{\sqrt{2}x}{w_x(z)}\right)\ \exp\left(\frac{ik_L}{2}\frac{x^2}{R_x(z)}\right)\ \exp\left(-i(m+\frac{1}{2})\phi_x(z)\right) \\ & \times\ \sqrt{\tfrac{\sqrt{2}}{w_y(z)}}\ \varphi_n\left(\tfrac{\sqrt{2}y}{w_y(z)}\right)\ \exp\left(\frac{ik_L}{2}\frac{y^2}{R_y(z)}\right)\ \exp\left(-i(n+\frac{1}{2})\phi_y(z)\right)\ . \qquad (1)\end{aligned}$$

Here, $\boldsymbol{r} = (x, y, z)$ is the position vector, ω_L the frequency of the monochromatic laser, $k_L = \omega_L/c = 2\pi/\lambda_L$ its wavenumber, and $\varphi_m(\xi) = H_m(\xi)\,\exp(-\xi^2/2)/\sqrt{2^m m!\sqrt{\pi}}$, $(m = 0, 1, 2, \ldots)$, with the Hermite polynomials H_m [37, 38, 39]. The wave front radii $R(z) = (z^2+z_R^2)/z$, the beam radii $w(z) = w_0\sqrt{1+z^2/z_R^2}$ with $w_0 = \sqrt{\lambda_L z_R/\pi}$, and the longitudinal Gouy-phase shifts [37, 38, 39], $\phi(z) = \arctan(z/z_R)$, are all parameterized by the beams' Rayleigh lengths z_R; strictly speaking by z_{R_x} and z_{R_y}, respectively.

In a configuration, such as that displayed in Fig. 1, one can generate [34, 36] a wide cylindrical atom-lens using a laser beam with an electric field composed of a suitable combination of odd modes

$$\Psi_{2J+1}(\boldsymbol{r}) = \sum_{j=0}^{J} c_{2j+1}\,\psi_{2j+1,0}(\boldsymbol{r})\ . \qquad (2)$$

Here, the beam is modulated in the x-direction whereas for the y-direction the purely Gaussian lowest order mode φ_0 is employed. Note that this allows us to make the lens 'thin' in the y-direction. With increasing cutoff, J, the superposition pattern becomes increasingly dephased due to the action of Gouy's phase [35], this will be further investigated in Section IV.

Following reference [38] the modes in Equation (1) yield an electric field which is polarized in the y-direction with a small contribution in the z-direction due to the tilt of wave fronts off the beam axis ($\hat{\mathbf{x}}, \hat{\mathbf{y}}, \hat{\mathbf{z}}$ are the unit-vectors and $\Re$ stands for real-part)

$$\boldsymbol{E}_{2J+1}(\boldsymbol{r}; t) = \Re\{[\hat{\mathbf{y}}\ \omega_L\ \Psi_{2J+1} + \hat{\mathbf{z}}\ ic\ \frac{\partial \Psi_{2J+1}}{\partial x}]e^{i(k_L z - \omega_L t)}\}\ . \qquad (3)$$

For beams that are not too tightly focused we neglect the transverse derivatives. The associated time-averaged light intensity distribution then has the form [38]

$$I_{2J+1}(\boldsymbol{r}) = \epsilon_0\ \left\langle \boldsymbol{E}_{2J+1}(\boldsymbol{r}, t)^2 \right\rangle \approx \frac{\epsilon_0}{2}\,\omega_L^2\,|\Psi_{2J+1}(\boldsymbol{r})|^2\ . \qquad (4)$$

B. Normalization and Intensity Scaling

With the normalized modes of Eq. (1) and assuming that the sum of the coefficients $\sum |c_{2j+1}|^2$ in Eq. (2) is unity we use the normalization

$$\int_{-\infty}^{\infty}\int_{-\infty}^{\infty} dx\, dy\, |\psi_{2J+1}(x,y,z)|^2 = \frac{2}{\epsilon_0\omega_L^2}\int_{-\infty}^{\infty}\int_{-\infty}^{\infty} dx\, dy\, I_{2J+1}(x,y,z)|^2 = 1\,. \tag{5}$$

Assuming validity of the Raman-Nath approximation of negligible transverse motion of the atoms ($(x,z) = const.$) [40], the atoms experience the y-integrated intensity distribution of the laser field given by

$$\bar{I}_{2J+1}(x,z) = \int_{-\infty}^{\infty} dy\, I_{2J+1}(\boldsymbol{r}) = \frac{\epsilon_0\omega_L^2}{2}\frac{\sqrt{2}}{w_x(z)}\ \left|\sum_{j=0}^{J}\varphi_{2j+1}(\frac{\sqrt{2}\,x}{w_x(z)})\ e^{-i(j+\frac{1}{2})\phi_x(z)}\right|^2 . \tag{6}$$

We note that this integrated intensity $\bar{I}$ of beams of fixed total power reduces inversely proportionally to their width w_{0x}, that is, their field amplitudes scale with $w_{0x}^{-1/2}$. Furthermore the field gradients diminish with w_{0x}^{-1}. This implies that the effective curvature of the integrated laser light intensity, $|\nabla\Psi|^2$, responsible for atomic focussing scales with w_{0x}^{-3}. We face an unfavourable cubic scaling with the beam width if we attempt to expand a laser beam transversally in order to widen the effective lens without weakening its refractive power. Additionally, as we will show below, pure modes have small useful areas to generate lenses, the combination of these two factors makes a pure mode approach unfeasible. It forces us to employ the mode superpositions studied here.

C. Optical Dipole Force

We assume that the interaction between atoms and the laser light is well described by a two-level scheme (excited state 'e' and ground state 'g') in rotating wave approximation with effective atomic line width Γ and resonance frequency $\omega = \omega_e - \omega_g$. This leads to the expression $I(\boldsymbol{r})\,\Gamma^2/(2I_S) = \Omega(\boldsymbol{r})^2$ for the Rabi-frequency Ω as a function of the ratio of the local laser intensity $I(\boldsymbol{r})$ and the transition's saturation intensity $I_S = \pi hc\Gamma/(3\lambda^3)$ [5, 26]. With sufficiently weak laser intensity I and sufficiently large detuning $\delta_\omega = \omega_L - \omega$ of the laser frequency ω_L from the atomic transition frequency ω, the AC-Stark shift gives rise to

a conservative optical dipole potential which, to first order in I/I_S, has the form [5, 41]

$$U_\omega \approx \frac{\hbar\,\Gamma^2}{8\,\delta_\omega}\frac{I(\boldsymbol{r})}{I_S}\,. \tag{7}$$

We can determine the atomic de Broglie wave number κ of atoms with mass M and initial kinetic energy $K_0 = (\hbar\kappa_0)^2/(2M)$ in terms of their kinetic energy K. Disregarding Doppler detuning, and assuming the validity of the Raman-Nath approximation ($K_0 \gg U_\omega$), this allows us to calculate the associated phase shift

$$\Delta\phi(x,z) \;\approx\; \int dy(\kappa(\boldsymbol{r}) - \kappa_0) = \frac{\sqrt{2MK_0}}{\hbar}\int dy(\sqrt{\frac{K}{K_0}} - 1) \tag{8}$$

$$\approx\; \frac{\sqrt{2MK_0}}{\hbar}\quad \int dy\,(\sqrt{1 - \frac{U_\omega}{K_0}} - 1) \;\approx\; \frac{-\sqrt{2M}\,\Gamma^2}{16\sqrt{K_0}I_S\delta_\omega}\,\bar{I}(x,z) \tag{9}$$

The dependence of Eq. (9) on the inverse kinetic energy implies that best performance is achieved for monochromatic atomic beams; the approximations are in accordance with the Raman-Nath assumption [40]. Work by Drewsen *et al.* [42] showed that, for an atom-lens, chromatic dispersion can be reduced by tilting the laser beam with respect to the passing atomic beam, but the focal plane would have to be tilted as well. Such a tilt, however, elliptically stretches out the atomic beam's point-spread function.

Aside from spherical aberrations, there are detrimental noise sources due to spontaneous emission of photons and light fluctuations. These tend to increase with increasing laser intensity but can be decreased by increased detuning [5] or through the use of more complicated optical level schemes [41]. Further discussion of their influences is beyond the scope of this paper.

III. CYLINDRICAL LENSES

According to eqns. (8) and (9) parabolic optical potentials give rise to parabolic atom-optical phase masks, as is required for 'perfect' atom lenses. In other words, we want the y-integrated electric field profile to depend linearly on the x-direction, see Fig. 2. In order to achieve this we integrate out the y-component, see Eq. (6), then Taylor-expand the field profile and finally choose the coefficients in Eq. (2) so as to cancel terms non-linear in x. Using the first $2J+1$ odd field modes all non-linear terms up to $(2J+1)^{\text{th}}$ order can be cancelled. The determination of the coefficients, c_{2j+1}, involves the solution of a linear equation system and is easily performed. For instance, for the third superposition

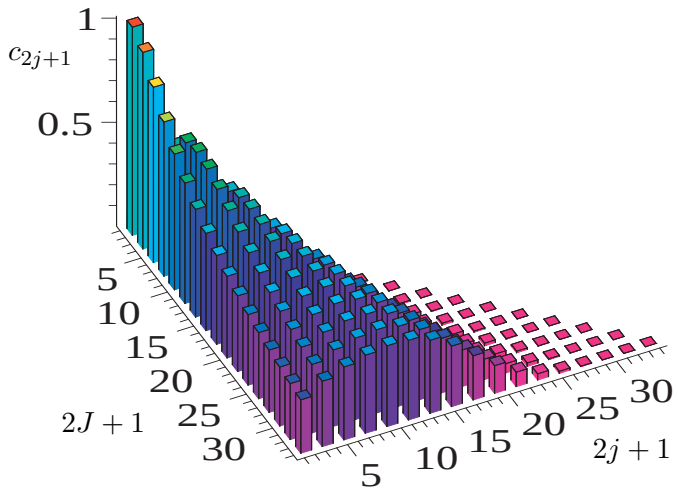

FIG. 3: (Color online) Amplitude coefficients c_{2j+1} of Hermite-Gauss superpositions Ψ_{2J+1} of up to 33^{rd} order modes ($2J+1 = 1, 3, \ldots, 33$).

field, Ψ_5, comprising Hermite-Gaussian modes $\psi_{1,0}$, $\psi_{3,0}$ and $\psi_{5,0}$, the relative strengths of the coefficients are $c_3 = c_1 18\sqrt{6}/71$ and $c_5 = c_1 2\sqrt{30}/71$. For a normalized superposition the coefficient c_1 should be chosen accordingly. The family of the first twelve normalized superpositions $\{\Psi_{2J+1}, 2J+1 = 1, 3, \ldots, 23\}$ is displayed in Fig. 2, the associated set of amplitude coefficients c_{2j+1} is shown in Fig. 3.

Mode-superpositions extend the "useful" linear part of the field profile yielding wider parabolic intensity profiles. Figure 4 demonstrates that the useful parabolic part in the focal intensity profile expands with the number of superposition modes $2J+1$ according to the $\sqrt{2J+1}$-scaling, expected for a harmonic oscillator [35]. Note, however, that the refractive power of the wider lenses is reduced (its atom-optical focal length is lengthened), because wider lenses have reduced transverse field gradients, see Fig. 2 and discussion following Eq. (6). In order to compensate for this loss of refractive power, we can increase the transverse field gradient through either laser beam focussing in the x-direction, or through an increase in laser beam power. Focussing in the y-direction makes no difference since only the integrated intensity $\bar{I}$ matters. In the next subsection we show how much the power has to be raised to keep the atomic lenses' refractive powers equal. Subsequently, in Section IV, we will investigate focussing in the x-direction; we will see that Gouy-dephasing constrains this focussing, the lenses must not be shrunken below a certain limit.

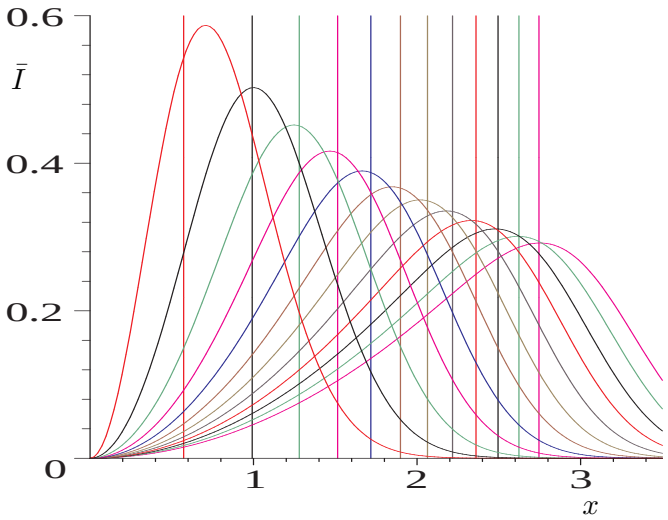

FIG. 4: (Color online) Integrated focal intensity profiles $\bar{I}(x,0)$ of Hermite-Gauss superposition beams comprising up to 23rd order modes, compare Fig. 2 (same units as in Fig. 2; vertical bars mark location of position $0.57 \cdot \sqrt{2J+1} \cdot w_{0x}$, confirming harmonic oscillator-scaling [35]).

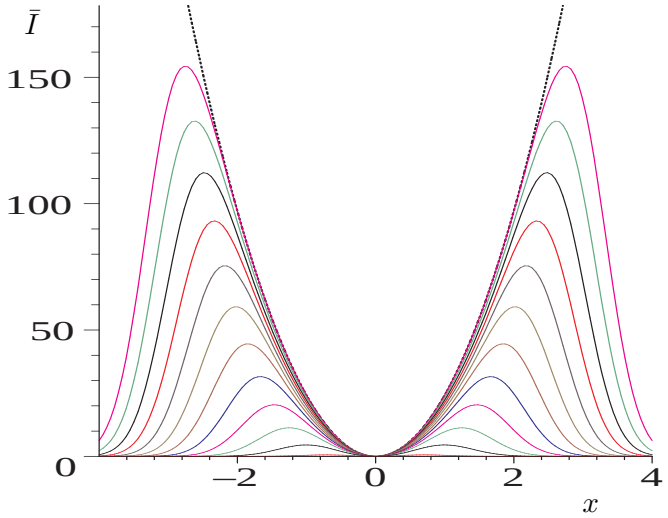

FIG. 5: (Color online) Integrated focal intensity profiles $\bar{I}(x,0)$ of Hermite-Gauss beams comprising up to 23rd order modes, compare Fig. 2 (same units as in Fig. 4; total beam power adjusted such that all profiles have same curvature at origin as the dotted line parabola).

A. Increased Beam Powers Compensates for Lenses Widening

If we increase the total beam power P_{2J+1} for wider beam profiles according to the ratios of the modes' transverse derivatives, $P_{2J+1} = P_1 |\partial_x \Psi_1(x,0,0)/\partial_x \Psi_{2J+1}(x,0,0)|^2$, the weakened gradient is power-compensated for by increased laser power. This way all optical potentials give rise to atom-lenses with equal refractive power, see Fig. 5. The necessary beam power

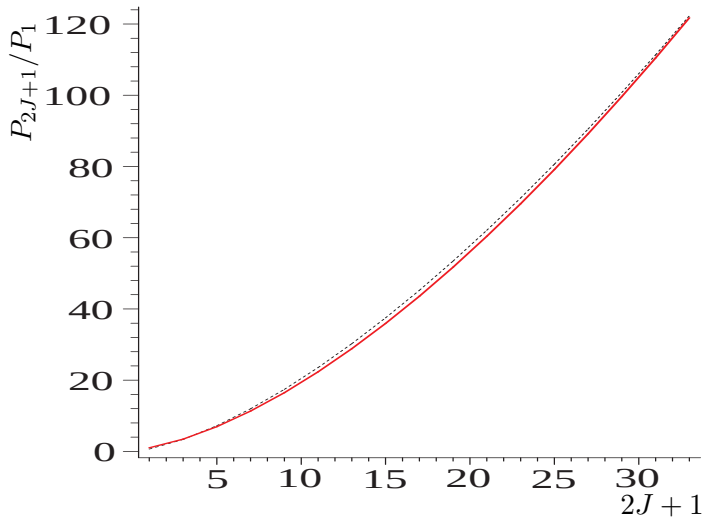

FIG. 6: (Color online) The increase in total beam power needed to achieve the power compensation described in the text and displayed in Fig. 5 as a function of mode number (solid red line) scales approximately like $\frac{20}{31} \cdot (2J+1)^{3/2}$ (dotted black line).

increase to achieve this compensation is sketched in Fig. 6. The power savings due to our multimode approach are quantified in Subsection III C.

B. Decreased Rayleigh-Lengths Compensate for Lenses Widening

Alternatively to the beam-power increases just discussed, we can keep the total beam power for all beams equal and shrink the higher-order superposition-beams' Rayleigh lengths through increased beam focussing in the x-direction. This also allows us to compensate for the gradient reduction observed in Fig. 2. The corresponding laser intensity profiles are displayed in Fig. 7 and lend themselves to an efficiency analysis of the invested laser power. The vertical bars in this figure mark the points, d_{2J+1}, where each intensity curve deviates from the enveloping parabola (dotted line) by 0.74 percent. They delineate the useful areas of the lenses. Beyond a deviation of 0.74%, spherical aberrations distort the atomic point-spread function of an imaged atomic beam too severely. The filled-in areas under the curves in Fig. 7 represent the laser power fraction contributing to the atom lens in each case. Higher-order superpositions clearly allow us to use the laser power much more efficiently. This is quantified in the next subsection.

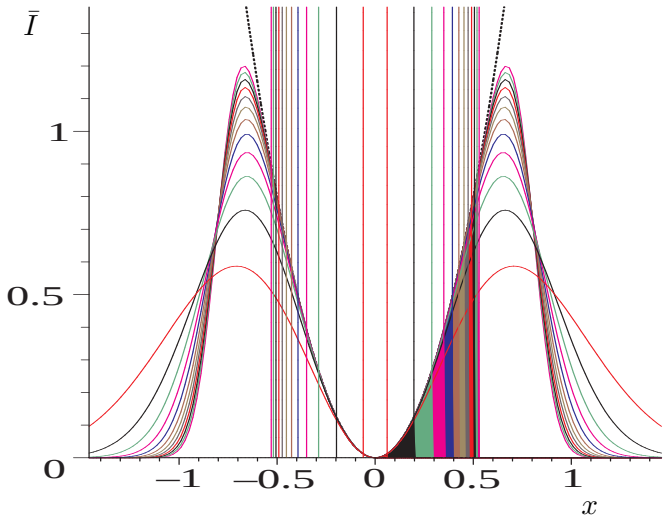

FIG. 7: (Color online) Integrated focal intensity profiles $\bar{I}(x,0)$ of Hermite-Gauss beams comprising up to 23rd order modes, compare Fig. 2, and their 0.74%-deviation marks, d_{2J+1}, which lie at relative positions $d_{2J+1}/d_1 = 1.00, 3.24, \ldots, 8.70$ from the origin, compare Table I (same units as in Fig. 2; in contrast to Fig. 5 total beam power normalized to unity, but Rayleigh lengths z_{Rx} readjusted such that all higher-order superpositions match up with curvature of the first mode case Ψ_1, see text).

C. Lens Quality and Power Savings

The 0.74%-criterion was extracted from the work by Gallatin and Gould [23] who considered, for example, the use of a 0.1 Watt laser detuned by roughly 40,000 linewidths. To achieve acceptable performance, the effectively useful beam area was found to be only some $2d_1$ =140 nm wide (for a laser beam with a $2w_{0x} = 2\mu$m waist diameter [23]). In other words, pure laser modes yield only a small useful window (in order to fulfill the 0.74%-deviation criterion only about $2d_1/(2w_{0x})$ =140 nm/2μm $\approx 7\%$ of a cylindrical lens diameter or only the central 0.49 percent area of a circular lens are useful). Most of the laser power is wasted in the wings if no suitable superpositions of higher-order modes are employed. In our case of a cylindrical lens based on the Hermite-Gaussian mode $\psi_{1,0}$, very similarly, approximately d_1/w_{0x} =6% of the width of the beam is useful, see Fig. 7. Additionally to the quantification of the useful area of the lenses, see Table I, this waste is meaningfully quantified through the determination of the fraction of power $\mathcal{E}_{2J+1}$ the laser beam contributes to the 'useful' part of the lens profile. We define it as the ratio of the laser energy contributing to the area

TABLE I: Lens Parameters d_{2J+1} and $\mathcal{E}_{2J+1}$, compare Fig.7

$2J+1$	1	3	5	7	9	11	13	15	17	19	21	23	25	27	29	31	33
d_{2J+1}/d_1	1.00	3.24	4.75	5.74	6.45	7.00	7.42	7.78	8.06	8.32	8.53	8.70	8.87	9.01	9.15	9.27	9.36
$\mathcal{E}_{2J+1}$ [%]	0.048	1.6	5.1	9.1	13	16	20	23	25	28	30	32	33	35	37	38	39
$\mathcal{E}_{2J+1}/\mathcal{E}_1$	1	34	107	190	269	344	411	472	526	576	620	662	699	735	766	795	825

between the deviation points $-d_{2J+1} < x < d_{2J+1}$, in terms of the total laser power, namely

$$\mathcal{E}_{2J+1} = \frac{\int_{-\infty}^{\infty} dy \int_{-d_{2J+1}}^{d_{2J+1}} dx\ I_{2J+1}(x,y,0)}{\int_{-\infty}^{\infty} dy \int_{-\infty}^{\infty} dx\ I_{2J+1}(x,y,0)}\,. \tag{10}$$

Figure 7 and Table I summarize and quantify our findings. Specifically, Table I allows us to compare values for a single-mode atom lens for which $\mathcal{E}_1 = 0.048\%$ with the superposition approach. For example, compared to mode Ψ_1 the relative power savings in case of superposition Ψ_{33} is 825, this translates into a power utilization of $\mathcal{E}_{33} = 0.048\% \times 825 = 39\%$. In general the details of this behaviour depend on the chosen quality criterion but the underlying scaling is straightforward to derive. The useful fraction of the laser beam is proportional to a linear integral over the intensity and therefore grows with the third power of the position of the deviation mark $\mathcal{E}_{2J+1}/\mathcal{E}_1 = (d_{2J+1}/d_1)^3$.

IV. SPHERICAL LENSES

We now want to investigate the constraints that arise when an identical copy of the laser beam that travels along the z-axis, see Fig. 1, is additionally sent along the x-axis such that their crossed configuration leads to the simultaneous application of two cylindrical lenses giving rise to the application of a spherical lens to the atomic beam. Either the laser beams are slightly displaced along the y-axis, or they are sufficiently detuned from each other such that despite their spatial overlap no harmful interference occurs [43].

Gouy's phase $\phi(z) = \arctan(z/z_R) \approx z/z_R$, introduces relative phases between the modes within each beam. Since the Gouy-phase varies strongest near the beam focus we have to consider its mode dispersive effects [35]. If the beam is very strongly focussed (small value of z_{R_x}) the dephasing away from the focus $z = 0$ is so rapid that non-linear aberrations

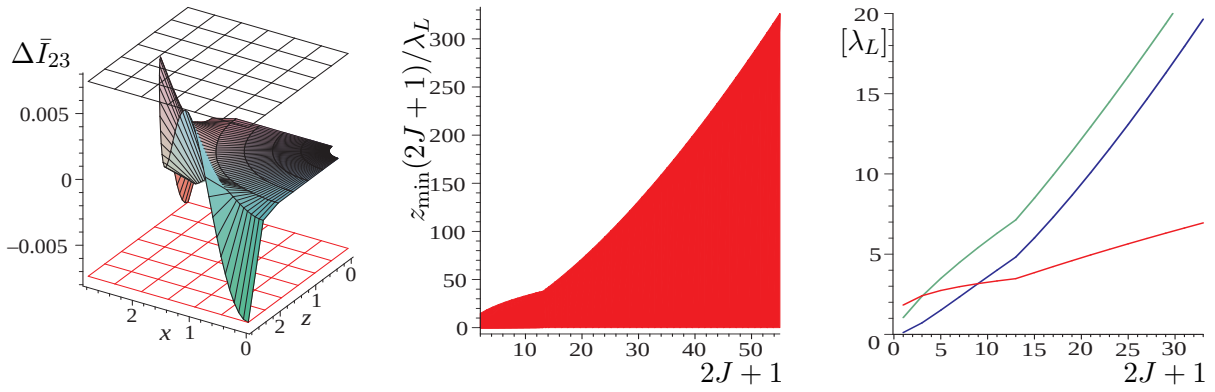

FIG. 8: (Color online) The left panel illustrates the behavior of the relative deviation of the intensity distribution $\Delta\bar{I}$ from zero as it approaches the 0.74%-deviation marks (top and bottom grid). Here, $\Delta\bar{I}_{23}$ is shown for the crossed configuration of two laser beams travelling along z and x-axis respectively. The value of the Rayleigh length z_{Rx} at which we find that the oscillatory behaviour of $\Delta\bar{I}$ along a constant radial perimeter just exhausts the upper and lower limits set by the deviation marks allows us to determine the associated value of $z_{\min}$. The latter is plotted as a function of maximum mode number, in the middle panel (the filled in red area is the forbidden area of too tightly focussed beams). The values of $z_{\min}(2J+1)$ in turn determine the positions of the turning points $0.57 \cdot \sqrt{2J+1} \cdot w_{0x}$ (top green line), the positions of the deviation-points d_{2J+1} (middle blue line) and the minimal beam widths $w_{0x}(2J+1)$ (bottom red line), depicted in the right panel in units of the laser's wavelength λ_L.

degrade the desired linear field profile over the width of the atom-lens. In other words, a lower limit for the Rayleigh lengths $z_{\min}(2J+1)$ as a function of the number of used modes '$2J+1$' has to be determined in order to guarantee moderate dephasing. Whereas the absolute values for this lower limit are hard to derive from first principles, we can still work out the correct scaling with the mode number:

The electric field is proportional to the superposition of the modes including the Gouy-phase factors; this can be approximated by $E_{2J+1} \propto \sum_{j=1,3,\ldots}^{2J+1} c_j \psi_j e^{ij\phi} \approx \sum_{j=1,3,\ldots}^{2J+1} c_j \psi_j (1 + ijz/z_{R_x})$. The expansion coefficients are positive and the wave functions are real at the focus $z = 0$. Since the first order term is purely imaginary the integrated intensity has to depend on z quadratically: $\bar{I}_{2J+1}(z) = \bar{I}_{2J+1}(0) \cdot [1 + \frac{z^2}{z_{Rx}^2} F_{2J+1} + \mathcal{O}(z^4)]$. The term F_{2J+1} has a complicated dependence on the number of modes, but, containing the square of sums of the form $\sum_{j=1,3,\ldots}^{2J+1} j c_j \psi_j$, is roughly proportional to $(2J+1)^2$. When we consider the

relative deviation of the intensity profile near the focus from the focal intensity distribution, $\Delta\bar{I} = \frac{\bar{I}(z)-\bar{I}(0)}{\bar{I}(0)}$, we find $\Delta\bar{I}_{2J+1} \propto \frac{z^2}{z_{R_x}^2} \cdot (2J+1)^2$. Additionally, we know that the widths of the superpositions scale roughly like those of the harmonic oscillator [35], see Fig. 4, namely $z \propto \sqrt{2J+1}$. For constant relative intensity deviations $\Delta\bar{I}_{2J+1}$ this implies $const. = \frac{\sqrt{2J+1}^2}{z_{R_x}^2} \cdot (2J+1)^2$ or $z_{R_x} \propto (2J+1)^{3/2}$. A numerical investigation, see Fig. 8, confirms $z_{\min}(2J+1) = 0.8 \cdot \lambda_L \cdot (2J+1)^{3/2}$ as a good estimate for a lower bound on z_{R_x}. This relationship has been checked numerically and holds for $15 < 2J+1 < 55$. There is no reason to believe deviations might occur for values of $2J+1 > 55$, but for small values of J the assumptions used in the derivation of the scaling law do not hold accurately, see Fig. 4. Instead, the expression $z_{\min}(2J+1) = 10.5 \cdot \lambda_L \cdot (2J+1)^{1/2}$ gives a much better estimate for $z_{\min}(2J+1)$ in the range of $1 < 2J+1 \leq 13$. These lower limits for z_{R_x} imply that the beam focus is several wavelengths wide and a posteriori confirms that the paraxial approximations hold for all cases discussed here, since the largest beam opening angle conforming with the lower limits presented here turns out to be roughly 7.5° for superposition Ψ_3.

V. CONCLUSIONS

For a possible experimental implementation of the ideas presented here it should be emphasized that throughout the use of a repulsive (blue-detuned) optical potential has been assumed since it allows us to build focussing lenses with a dark center reducing detrimental spontaneous emission noise. Equivalent logic applies to 'concave' atomic lenses which would best be implemented in red detuning, with dark centers as well.

The Raman-Nath assumption becomes progressively worse the larger the numerical aperture of a lens. Trajectory simulations show a 'downhill' drift of atomic paths that can partly be compensated for by slightly weakening the rise of the potential through the suitable subtraction of higher-order terms that lead to slight non-harmonic modifications of the lens, improving its performance. Clearly, if such fine-tuning is considered, the approximations underlying Eq. (4) and Eq. (7) might not be permissible. These considerations are beyond the scope of this paper.

The techniques for the coherent superposition of laser modes have been experimentally demonstrated, see e.g. references [34, 36] and citations therein. We have found here that using the mode-superposition approach allows for very considerable laser power savings and

lenses can be made wider than is possible with pure modes. We come to the conclusion that for the design of atomic lenses, based on the optical dipole force, it is possible and necessary to coherently superpose suitable laser modes in order to create wide thin parabolic lenses with large numerical apertures.

Obviously the approach presented here can be applied for the manipulation of stationary atomic clouds just as well as for atomic beams [44, 45].

Acknowledgments

I would like to thank Neil Oxtoby for careful reading of the manuscript and the referees for their very helpful comments.

---

[1] D. Meschede and H. Metcalf, J. Phys. D: Appl. Phys. **36**, R17 (2003).

[2] T. Ito and S. Okazaki, Nature **406**, 1027 (2000).

[3] R. B. Doak, R. E. Grisenti, S. Rehbein, G. Schmahl, J. P. Toennies, and C. Wöll, Phys. Rev. Lett. **83**, 4229 (1999).

[4] B. Ward, J. Notte, and N. Economou, Photonics Spectra **41**, 68 (2007).

[5] H. J. Metcalf and P. van der Straten, *Laser Cooling and Trapping* (Springer, New York, 1999).

[6] J. E. Bjorkholm, R. R. Freeman, A. Ashkin, and D. B. Pearson, Phys. Rev. Lett. **41**, 1361 (1978).

[7] B. Holst and W. Allison, Nature **390**, 244 (1997).

[8] D. Barredo, F. Calleja, P. Nieto, J. J. Hinarejos, G. Laurent, Amadeo, D. Farías, and R. Miranda, Advanced Materials **20**, 3492 (2008).

[9] D. W. Keith, M. L. Schattenburg, H. I. Smith, and D. E. Pritchard, Phys. Rev. Lett. **61**, 1580 (1988).

[10] O. Carnal, M. Sigel, T. Sleator, H. Takuma, and J. Mlynek, Phys. Rev. Lett. **67**, 3231 (1991).

[11] H. Oberst, D. Kouznetsov, K. Shimizu, J. Fujita, and F. Shimizu, Phys. Rev. Lett. **94**, 013203 (2005).

[12] H.-R. Noh, K. Shimizu, and F. Shimizu, Phys. Rev. A **61**, 041601 (2000).

[13] M. Drndić, K. S. Johnson, J. H. Thywissen, M. Prentiss, and R. M. Westervelt, Appl. Phys. Lett. **72**, 2906 (1998).

[14] W. G. Kaenders, F. Lison, I. Müller, A. Richter, R. Wynands, and D. Meschede, Phys. Rev. A **54**, 5067 (1996).

[15] E. Marechal, B. Laburthe-Tolra, L. Vernac, J. C. Keller, and O. Gorceix, Appl. Phys. B **91**, 233 (2008).

[16] D. A. Smith, A. S. Arnold, M. J. Pritchard, and I. G. Hughes, J. Phys. B: At. Mol. Opt. Phys. **41**, 125302 (2008).

[17] E. A. Hinds and I. G. Hughes, J. Phys. D: Appl. Phys. **32**, R119 (1999).

[18] V. I. Balykin, V. V. Klimov, and V. S. Letokhov, Optics and Photonics News **16**, 44 (2005).

[19] M. Mützel, M. Müller, D. Haubrich, U. Rasbach, D. Meschede, C. O'Dwyer, G. Gay, B. V. de Lesegno, J. Weiner, K. Ludolph, et al., Appl. Phys. B **80**, 941 (2005).

[20] H. Ito, K. Yamamoto, A. Takamizawa, H. Kashiwagi, and T. Yatsui, J. Opt. A: Pure Appl. Opt. **8**, S153 (2006).

[21] L. E. Helseth, Phys. Rev. A **66**, 053609 (2002).

[22] A. Gangat, P. Pradhan, G. Pati, and M. S. Shahriar, Phys. Rev. A **71**, 043606 (2005).

[23] G. M. Gallatin and P. L. Gould, J. Opt. Soc. Am. B **8**, 502 (1991).

[24] J. J. McClelland and M. R. Scheinfein, J. Opt. Soc. Am. B **8**, 1974 (1991).

[25] G. Timp, R. E. Behringer, D. M. Tennant, J. E. Cunningham, M. Prentiss, and K. K. Berggren, Phys. Rev. Lett. **69**, 1636 (1992).

[26] V. Natarajan, R. Behringer, and G. Timp, Phys. Rev. A **53**, 4381 (1996).

[27] K. S. Johnson, J. H. Thywissen, N. H. Dekker, K. K. Berggren, A. P. Chu, R. Younkin, and M. Prentiss, Science **280**, 1583 (1998).

[28] M. Mützel, S. Tandler, D. Haubrich, D. Meschede, K. Peithmann, M. Flaspöhler, and K. Buse, Phys. Rev. Lett. **88**, 083601 (2002).

[29] B. Dubetsky and P. R. Berman, Phys. Rev. A **58**, 2413 (1998).

[30] M. Mützel, U. Rasbach, D. Meschede, C. Burstedde, J. Braun, A. Kunoth, K. Peithmann, and K. Buse, Appl. Phys. B **77**, 1 (2003).

[31] V. V. Klimov and V. S. Letokhov, J. Mod. Opt. **42**, 1485 (1995).

[32] P. Barberis and B. Rohwedder, Phys. Rev. A **67**, 033604 (2003).

[33] G. Ritt, C. Geckeler, T. Salger, G. Cennini, and M. Weitz, Phys. Rev. A **74**, 063622 (2006),

arXiv:cond-mat/0512018.

[34] O. Steuernagel, E. Yao, K. O'Holleran, and M. Padgett, J. Mod. Opt. **52**, 2713 (2005).

[35] O. Steuernagel, Am. J. Phys. **73**, 625 (2005).

[36] C. Maurer, A. Jesacher, S. Fürhapter, S. Bernet, and M. Ritsch-Marte, New J. Phys. **9**, 78 (2007).

[37] A. E. Siegman, *Lasers* (Oxford Univ. Press, Oxford, 1986).

[38] H. A. Haus, *Electromagnetic Noise and Quantum Optical Measurements* (Springer, Heidelberg, 2000).

[39] F. Pampaloni and J. Enderlein (2004), arXiv:physics/0410021.

[40] H. Wallis, Phys. Rep. **255**, 203 (1995).

[41] J. J. Hope and C. M. Savage, Phys. Rev. A **53**, 1697 (1996).

[42] M. Drewsen, R. J. C. Spreeuw, and J. Mlynek, Opt. Commun. **125**, 77 (1996).

[43] M. T. DePue, C. McCormick, S. L. Winoto, S. Oliver, and D. S. Weiss, Phys. Rev. Lett. **82**, 2262 (1999).

[44] O. Steuernagel, J. Opt. A: Pure Appl. Opt. **7**, S392 (2005).

[45] D. R. Murray and P. Öhberg, J. Phys. B: At. Mol. Phys. **38**, 1227 (2005).